JBIC Journal of Biological Inorganic Chemistry (2022) 27:155–173
https://doi.org/10.1007/s00775-021-01918-z

ORIGINAL PAPER

Gamma irradiation effectuality on the antibacterial and bioactivity behavior of multicomponent borate glasses against methicillin-resistant *Staphylococcus aureus* (MRSA)

W. M. Abd-Allah[1] · Rasha Mohammad Fathy[2]

Received: 14 September 2021 / Accepted: 14 November 2021 / Published online: 22 January 2022

Abstract

Abstract Recently some borate bioactive glasses have been discovered to have an antibacterial effect when interacting with pathogenic bacteria. In this study, borate bioactive glasses (BG) doped with metal oxide (MO) ZnO, TiO_2, TeO_2, and CeO_2 (encoded BG-Zn, BG-Ti, BG-Te, and BG-Ce, respectively) were prepared using the melt-quench method and have been characterized before and after gamma irradiation at 25.0 kGy. X-ray diffraction was performed to recognize the amorphous phases of all samples. Infrared absorption of glasses confirms vibrational bands in their wave number according to mixed main triangular and tetrahedral borate groups. After immersion in the simulated body fluid (SBF) solution, two characteristic peaks are generated indicating the bioactivity of the studied glasses through the formation of hydroxyapatite. SEM micrographs of glass after immersion display that the crystalline phases are identified to be more distinct in different shapes because of the multi-composition involved. The antibacterial activity of borate glasses was assessed against methicillin-resistant *Staphylococcus aureus* (MRSA) ATCC 6538. The antibacterial results showed that BG-Te was the most efficient against *S. aureus* ATCC 6538. Furthermore, BG-Te reduced biofilm production (79.23%) at the concentration of 20.0 mg/mL. (BG-Te) at 20.0 mg/mL significantly decreased the viability percent, cell count, protein content, and protease activity of *S. aureus* cells. BG-Te presents powerful activity against bacterial infections. It was necessary to equilibrate the antibacterial efficiency with the biocompatibility, so the MTT assay confirmed that BG-Te has low cytotoxicity on the human fibroblast cells (WI-38). It is expected that borate bioglass contained TeO_2 could be a promising biomaterial for bone tissue engineering.

✉ Rasha Mohammad Fathy
rasha.elhadad@eaea.org.eg; rashafathy82@gmail.com

[1] Radiation Chemistry Department, National Centre for Radiation Research and Technology (NCRRT), Egyptian Atomic Energy Authority (EAEA), P.O Box 29, Nasr City, Cairo, Egypt

[2] Drug Radiation Research Department, National Center for Radiation Research and Technology (NCRRT), Egyptian Atomic Energy Authority, Nasr City, P.O Box 29, Cairo, Egypt

Graphical abstract

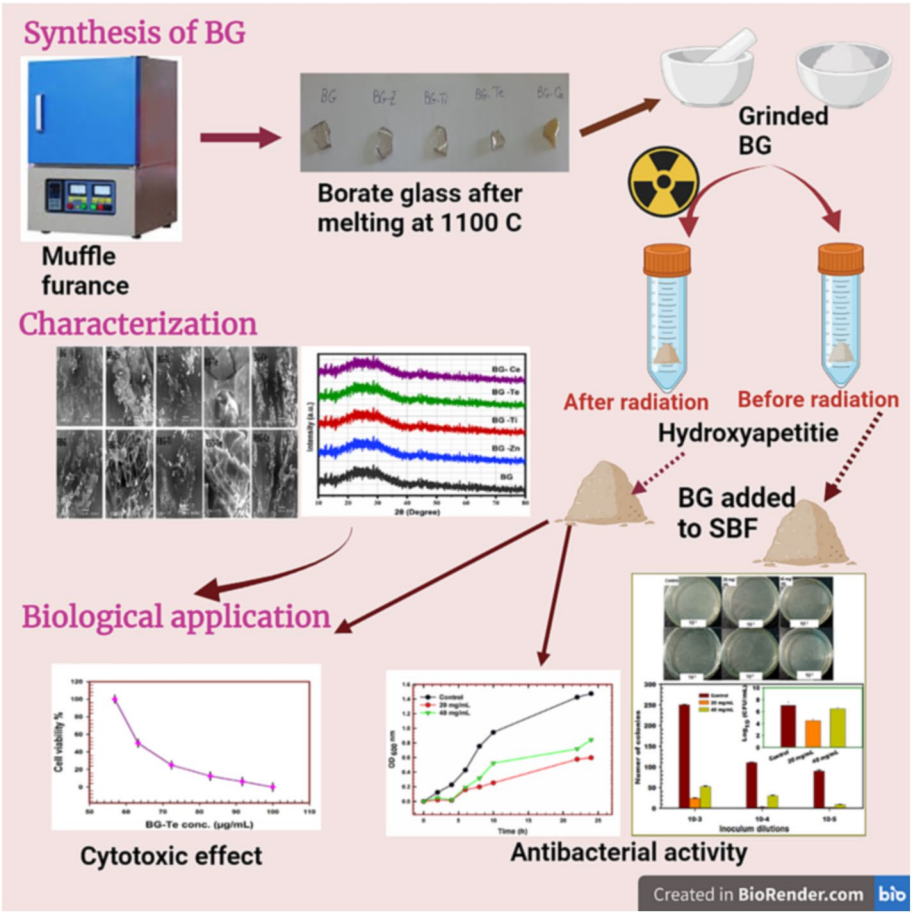

Keywords Borate bioglass · Gamma rays · *Staphylococcus aureus* · Antibacterial · Antibiofilm · Cytotoxicity

Introduction

Borate glasses have several benefits rather than silicate bioactive glasses, including a faster and nearly complete conversion to hydroxyapatite [1]. Bioactive glass is a group of biocompatible materials that may be used to solve the hazards of implant injection caused by metal or plastic surgery [2]. In recent times, Bone binding or antibacterial metal oxides in the composition of various borate glasses have been the target of numerous studies [3].

Borate bioactive glasses improve bone formation more quickly than Hench's silicate Bioglass by stimulating the proliferation and differentiation of human mesenchymal stem cells [4].The high modifier concentrations create lots of non-bridging oxygens NBOs which subsequently disrupt the connection of the borate network. This disruption makes the developed borate glass extremely sensitive to chemical degradation. These NBOs are ideal sites for accelerating the corrosion process [5].

In some instances, for causes that are not understood, it becomes significantly difficult to control bacterial infections [6]. *S. aureus* is a gram-positive bacterium that is commonly present in nature. Because of the susceptibility of clinical pathogens and the dense community, people infected with *S. aureus* suffer from chronic illness. To mitigate this trouble, clinicians and scientists have studied the pathogenic mechanism of *S. aureus*, which is recently become very resistant to vancomycin. The restricted use of drugs in controlling antimicrobial-resistant microbes may cause the appearance of more resistant strains [7]. To destroy or inhibit the growth of bacteria, bioactive drugs such as tetracycline and ampicillin are commonly employed [8]. The antibacterial activity of the bioactive glass was studied against a wide spectrum of bacteria growing aerobically and an aerobically. Furthermore, "needle-like" sharp glass fragments may cause hollows and holes in bacterial cell walls, allowing antimicrobial medications to enter the bacterial cytoplasm [9]. Many researchers [10, 11] investigated the antibacterial properties of metal

ions (Ag^{+}, Cu^{2+}, Zn^{2+}) in a variety of glasses for use against bacteria and fungi. Certain bacteria cause osteomyelitis, 80 percent of them are multi-drug resistant (MRSA) and methicillin-resistant *S. aureus* [12, 13]. Kung et al. [14] examined the antibacterial activity of Ag-contained bioactive glass microspheres against the common strains of *S. aureus* (ATCC6538 and ATCC 25923).

Extrinsic factors that are like (shock, operations, and bone metal fittings) and intrinsic factors (causing microbial infections, body feebleness, malnutrition, and deficiency of immunity) may facilitate the bacterial infections in humans [15]. Antibiotics are often used to destroy or slow bacterial growth. However, bacterial resistance to antibiotics has emerged as a result of their widespread and frequently inappropriate usage. Furthermore, taking a high dose of antibiotics might have negative side effects and induce unacceptable toxicity [16].

The treatment of implant-embedded osteomyelitis using biomaterials has received a lot of attention and has been thoroughly researched. Therefore, there is a great necessity to improve novel and efficient strategies to resist osteomyelitis [17]. The bioactive glass is known to have powerful antibacterial characteristics. These antimicrobial capabilities, along with bioglass' osteostimulative and osteoconductive properties, make it a suitable treatment for osteomyelitis [18]. The bioactive glasses are effective against the majority of common bacteria that cause osteomyelitis, creating an environment free of microbial contamination [19].

Sterilization is described as the process that effectively kills or reduces almost of microorganisms like fungi, bacteria, and viruses. There are different methods of sterilization such as dry ethylene oxide (EtO), gas plasma (H_2O_2), heat, pressured vapor, formaldehyde, peracetic acid, and gamma irradiation. The selection of any sterilization method mainly depends on materials and devices that does not cause harm [20].

Borate bioactive glasses doped with metallic elements are the point of interest in this study. This paper was aimed to investigate the impact of different metal oxides and gamma irradiation on the biocompatibility and the antibacterial activities of borate bioglass. The antibacterial efficiency of the aforementioned materials against methicillin-resistant *S. aureus* (MRSA) ATCC 6538 was studied to establish superior performance for medical and surgical applications. Moreover, MTT assays are used to complete in vitro biological studies.

Materials and methods

Glass samples in Table 1 with the nominal compositions (45 B_2O_3 -24.5 CaO- 24.5 Na_2O- 6 P_2O_5) in mol% with additions of MO (2%) either ZnO, TiO_2, TeO_2, and CeO_2. The raw materials were H_3BO_3 from B_2O_3. Ammonium di-hydrogen phosphate for P_2O_5, Na_2O, CaO come from Sodium and calcium carbonates, in the same time MO was introduced as such as, Tellurium ions from metal oxide (99.99% purity, Alfa). The produced mixtures were prepared by the melt-quench technique in porceline crucible at 1150–1200 °C for 2.0 h, then annealing at 450 °C.

X-ray diffraction analysis

The glass samples were investigated by Bruker D8 (Germany) adopting Cu radiation with Ni-filter at a speed of 2o 2Θ/min. The reference data of the interpretation of X-ray were obtained from American Standard for Testing Materials (ASTM) through the measurements at the room temperature and under constant operating conditions.

Structural characterization through FTIR spectral analysis

Fourier transform infrared (FTIR) absorption spectra of the glasses were measured at room temperature before and after immersion in the SBF solution for the specified times. FTIR spectrometer (type (JASCO FT/IR-300E spectrophotometer, Japan) was used in the wavenumber range 2000–400 cm^{-1}. The FTIR measurements were immediately done after the preparation of the discs to avoid moisture attacks. The exact measurements were repeated after the immersion of the glass and irradiated glass in the SBF solution for a specified time (2.0 weeks), the immersed powdered samples were spread on filter papers and kept in desiccators for 24 h for dryness.

Table 1 Chemical composition of the prepared glass samples

Glass code	Mol %				Added metal oxide	Glass code after irradiation
	B_2O_3	Na_2O	CaO	P_2O_5		
BG	45	24.5	24.5	6	0	RBG
BG-Zn	45	24.5	24.5	6	2% ZnO	RBG-Zn
BG-Ti	45	24.5	24.5	6	2% TiO_2	RBG-Ti
BG-Te	45	24.5	24.5	6	2% Te_2O_3	RBG-Te
BG-Ce	45	24.5	24.5	6	2% CeO_2	RBG-Ce

Weight loss measurements

1.0 g of the glass grains was immersed in 100 mL of SBF solution in a 250 mL polyethylene beaker fitted in water bath regulated at 37 °C for 2 weeks. The weight loss after immersion was calculated for each sample.

Scanning electron microscopic investigations (SEM)

Morphological investigations of the surfaces of the glasses were carried out after immersion in the SBF solution using an SEM model Jeol-JSM5400 with accelerating voltage of 30 kV. All samples studied were coated with surface layer of gold for morphological investigations.

Gamma irradiation procedure

The gamma ray source used in irradiating glasses during the whole experimental work was ^{60}Co gamma cell (2000 Ci) with a dose rate 1.52 kGy/ h at 30 °C. The glass samples were placed in the gamma cell in the manner that each sample was subjected to the same gamma dose.

Agar well diffusion method

The agar well diffusion procedure is broadly used to estimate the antimicrobial activity of different materials [21]. The agar well diffusion test was carried out according to Fathy et al. [22] to assess the antibacterial influence of multicomponent borate glass against methicillin-resistant *S. aureus* (MRSA) ATCC 6538. The *S. aureus* was kindly obtained from The Drug Microbiology Lab., National Center for Radiation Research and Technology (NCRRT), Egyptian Atomic Energy Authority. Firstly, *S. aureus* was incubated in a nutrient broth medium overnight for enhancing the growth of bacteria. After the incubation for 24 h, *S. aureus* was incubated for 2.0 h to reach the lag phase. The *S. aureus* suspension was modified to standard 0.5 McFarland's concentration that equal an inoculum size of 1.0×10^8 CFU/mL. The surface of the nutrient agar plates was inoculated with 100 µL of the bacterial inoculum. The volume of 1.0 mL of the borate glass solutions (BG, BG-Zn, BG-Ti, BG-Te, and BG-Ce) at concentrations of 10.0, 20.0, and 40.0 mg/mL was introduced into the wells (the diameter, 8 mm) punched on the agar surface with a sterile cork borer. The agar plates were then incubated at 37 °C for 24 h. All experiments were performed in triplicates and the inhibition zones (ZOI) were evaluated in mm as mean values. *S. aureus* was inoculated on the surface of the nutrient agar medium.

Minimum inhibition concentration

Minimum Inhibitory Concentration (MIC) and Minimum Bactericidal Concentration (MBC) of BG-Te and BG-Ti against *S. aureus* ATCC 6538 were determined by the macro-dilution method following Salem et al. [23]. *S. aureus* ATCC 6538 inoculum was diluted in a nutrient broth medium to prepare the bacterial cells concentration of 10^8 CFU/mL. The BG-Te and BG-Ti concentrations were provided as 25.0, 12.5, 6.25, 3.12, and 1.56 mg/mL. A volume of 100 µL of *S. aureus* ATCC 6538 suspensions (10^8 CFU/mL) was introduced to the tubes with BG-Te and BG-Ti dilutions. After a 24-h incubation period at 37 °C, the turbidity of the bacterial growth was observed. The MIC was recognized as the lowest BG-Te and BG-Ti concentrations that could inhibit the noticeable *S. aureus* ATCC 6538 growth after 24 h of incubation. Additionally, MBC was expressed as the concentrations of BG-Te and BG-Ti that completely exclude all the bacterial after 24 h.

The antibiofilm activity of the borate glass against *S. aureus* ATCC 6538

The BG-Te (10.0, 20.0, and 40.0 mg/mL) experimented for their antibiofilm potential against *S. aureus* ATCC 6538 by test tubes technique as reported by El- Shazly et al. [24]. 10.0 µL of 0.5 McFarland (1.0×10^8 CFU/mL) of *S. aureus* ATCC6538 was inoculated in the 5.0 mL nutrient broth tubes. The volume of 0.5 mL of BG-Te (10.0, 20.0, and 40.0 mg/mL) was injected into the nutrient broth tubes. The equivalent volume of water was injected into the control tube. All test and control tubes were incubated overnight at 37 °C. After the incubation time, the media of all tubes were excluded. Phosphate buffer saline (PBS, pH 7) was added to the tubes and finally dehydrated. The volume of 5.0 mL of sodium acetate (3.0%) was employed to preserve the adhering bacterial films for 10.0 min then rinsed with water. The bacterial biofilms were dyed with crystal violet (0.1%) for 15.0 min after that the residue of the dye was discarded by washing with de-ionized water. Ethanol (2.0 mL) was used to dissolve the crystal violet dye. The *S. aureus* biofilms settled on the tubes' surfaces and bottoms. The biofilms were appraised by UV–Visible spectrophotometer at $\lambda = 570$ nm. The inhibition percentage was valued by Eq. 1.

$$\text{Inhibition}\% = \left(OD_c - OD_t/OD_c\right) \times 100 \quad (1)$$

where; OD_c denotes the control's optical density (without glass) and the optical density of the treatment is OD_t.

Kinetics of *S. aureus* ATCC 6538 growth

The impact of BG-Te on the kinetices of *S. aureus* ATCC 6538 was investigated using the Huang et al. method [25]. *S. aureus* suspension was cultured in a nutrient broth medium for 24 h at 37 °C. A 0.5 McFarland inoculum of *S. aureus* was prepared in test tubes containing 9.5 mL of a nutrient broth medium. 0.5 mL of 20.0 and 40.0 mg/mL concentrations of BG-Te were added to the tubes of the bacterial suspension then incubated at 37 °C. For preparing the blank sample, 0.5 mL of distilled H_2O was supplemented equivalent to the volume of BG-Te. Aliquots of 1.0 mL of the for *S. aureus* ATCC 6538 growth medium were taken at time intervals of 0.0, 2.0, 4.0, 6.0, 12.0, and 24 h. Using a UV–visible spectrophotometer, the optical density of the samples was observed at $\lambda = 600$ nm. Growth curves were analyzed by plotting the absorbance at $\lambda = 600$ nm against the time (h).

Viable cell counts of *S. aureus* ATCC 6538

The antibacterial activity of BG-Te on the viability of *S. aureus* ATCC 6538 was evaluated regarding to Kung et al. [26]. The bacteria suspension count was adjusted to 0.5 McFarland standards. The BG-Te at concentrations of 20.0 and 40.0 mg/mL were prepared and used stalk solutions. A control sample was prepared without addition of BG-Te. Tenfold serial dilutions of each stock solution were qualified to obtain dilutions from 10^{-1} to 10^{-5}. Tubes were incubated at 37 °C for 18 h. The volume of 100 µL from the last three dilutions was spread on nutrient agar plates then incubated at 37 °C for 24 h. The test was repeated in triplicate. For every dilution, colonies were enumerated and the CFU/mL was estimated. Viable cell number reduction was expressed as $\log_{10}$ CFU/mL.

Biochemical analysis's

Preparation of *S. aureus* ATCC 6538 supernatant

The *S. aureus* ATCC 6538 inoculum was inoculated in a nutrient broth medium then incubated overnight at 37 °C. The bacterial cells were harvested by centrifugation at 10,000 rpm for 10.0 min. The wet and dry weights of cell pellets were estimated. *S. aureus* supernatant was kept at refrigerated condition until further use in the biochemical parameters studied.

Protein content assay of *S. aureus* ATCC 6538

S. aureus supernatants of blank (without borate glass) and BG-Te (20.0, 40.0 mg/mL) were prepared. An aliquot 3.0 µL of each supernatant was diluted to 5.0 mL with 50.0 mM sodium phosphate buffer (pH 7). The supernatants were mixed strongly with 5.0 mL of Coomassie brilliant blue (CBB) G-250. The absorbance was read at $\lambda = 595$ nm against a reagent blank [27]. Protein content was assessed using the bovine serum albumin (BSA) standard and represented in (mg/mL).

Alkaline protease activity of *S. aureus* ATCC 6538

Protease activity was estimated by the procedure of Kalwasińska et al [28] utilizing a substrate of azocasein. In a 100 mMTris-HCl buffer (pH 8.8), 300 µL of *S. aureus* ATCC 6538 supernatant that was previously treated with BG-Te (20.0 and 40.0 mg/mL) was mixed with 300 µL of azocasein (0.5 %). Samples were incubated at 40 °C for 30 min. The reaction was blocked using 600 µL of 10 % trichloroacetic acid (TCA). The solutions were centrifuged at 10,000 rpm and the absorbance was estimated at 420 nm. The standard curve of azocasein was plotted at concentrations of 0.3–1.5 mg/mL against the correspondent readings.

Appraisal of the cytotoxicity of BG-Te

Cell culture

This analysis was performed at the Holding Company for Biological Products and Vaccines (VACSERA), Cairo, Egypt. Human fibroblast cells (WI-38) were cultured in Dulbecco's modified eagle's medium supplied by fetal bovine serum (10%) and 1% of antifungal/antibacterial solution. The cells were incubated at 37 °C with 5% CO_2. BG-Te was brought into suspensions with concentrations of 100, 50, 25, 12.5, 6.25, and 0.0 µg/mL.

Cell viability assay [29]

The WI-38cells (1×10^5 cells/mL) were seeded by 100 µL/well on a 96- well plate then incubated at 37 °C for 24 h. After the overnight incubation, the cell monolayer was washed twice. 0.1 mL of the Two-fold dilutions of the BG-Te was poured in wells. The culture without borate glass was applied as a negative control. Plates were incubated at 37 °C before the examination. Twenty microliters of MTT solution (5.0 mg/mL in PBS) were added to each well, shake at 150 rpm for 5.0 min, and then incubated at 37 °C for 4 h to permit the development of formazan crystal. After incubation, 200 mL of dimethyl sulfoxide (DMSO) was pipetted into every well for dissolving the formazan. Each experiment

was established in triplicate. Optical density (O.D.) was read spectrophotometrically at 560 nm. The cell viability percentage was determined by the subsequent equation Eq. 2:

$$\%\text{Cell viability} = \left[\frac{(\text{Sample absorbance} - \text{blank absorbance})}{(\text{control absorbance} - \text{blank absorbance})}\right] \times 100 \quad (2)$$

Statistical analysis

IBM Corp (V. 24, Armonk, NY: USA) was applied for analyzing data obtained from study using one way ANOVA followed by Ducan`s multiple range test.

Results and discussion

X-ray diffraction

X-ray diffraction (XRD) patterns of all compositions for the prepared glass systems are shown in Fig. 1. XRD show hump peak. This approves the non-crystalline nature of the prepared glasses.

FTIR absorption measurements of glasses before and after immersion in SBF

The studied base glass composition includes high B_2O_3 content, collective alkali, alkaline earth oxides, and P_2O_5. This composition consists of triangular and tetrahedral units of borate groups in separate specific wave numbers and some phosphate groups, providing the lattice composite or mixed pattern of various groups. The spectra are represented into the following three regions:

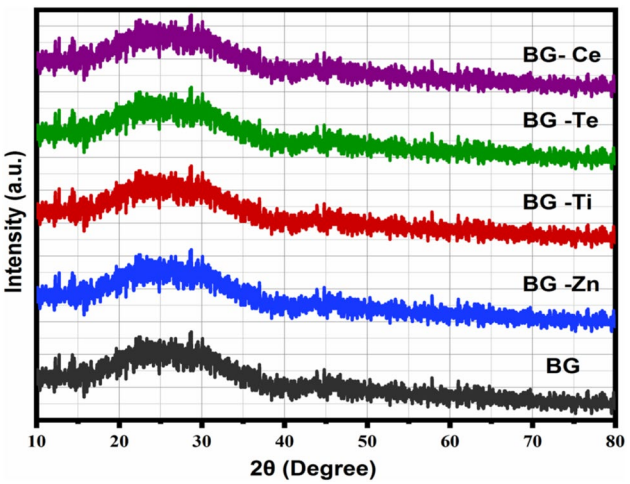

Fig. 1 X-ray diffraction patterns of prepared glasses system

1. 1200–1500 cm^{-1} which belongs to B–O stretching vibrations of triborate BO_3 units.
2. 850–1200 cm^{-1} which owing to B–O stretching vibrations of tetraborate BO_4 units.
3. 600–800 cm^{-1} related to bending vibrations of different borate sections.

The IR absorption spectra of the un-doped glass system were explained in Fig. 2a; therefore, the identified mean characteristic peaks in the glass systems were detected at the specific wave numbers. The prominent band in the region closely at 420 and 470 cm^{-1} were related to specific vibrations of metal cations bonds [30]. The small band at 560 may be assigned to B–O–B vibration [2]. The shoulder band at 630 cm^{-1} is ascribed to the vibrations bending of various borate groups. The IR analysis recognized the prominent peak at 700 cm^{-1} is matched to B–O–B linkages bending in the borate network [3].

Many bands that are near to each other at 950, 1010, and 1060 cm^{-1} are from the bonds of oxygen connecting the adjacent coordination tetrahedra of numerous components, developing the network [4, 5], or correlated to tetracoordinated borate vibrations (BO_4) [3]. The small band at 1160 cm^{-1} is due to the B–O asymmetric stretching of tetrahedral BO_4 units and diborates joining in pentaborate groups. The medium band that appeared at 1250 cm^{-1} can be assigned to boroxyl rings and H_2O molecular vibrations [6]. A strong peak at 1390 cm^{-1} is attributed to the vibration of the oxygen bridge between the BO_3 and BO_4 groups [7]. The shoulder band at 1460 cm^{-1} can be related to vibrations of water molecules [3]. An additional IR peak at 1620 cm^{-1} is related to OH vibration of water [2, 8].

Interpretation of the FTIR spectra of the multi-component borate glasses

A comparison of IR spectra of the BG-Zn, BG-Ti, BG-Te, and BG-Ce glass samples reveal nearly related vibration peaks as the un-doped specimen which may be due to similar composition of the glass matrix, but with a minor change in their intensity; especially with ZnO, TiO_2, and Ce_2O_3 doped. From Fig. 2a, the spectra show some changes through the increase or decrease in some bands and comparing their spectra with the parent glasses. Generally, that can be explained that increasing or decreasing in intensity of bands occur according to the transformation of BO_4 to BO_3 and vice versa with the potency of building bridging and non-bridging oxygen's [8, 10]. On the other hand, the differences are not declared by observations from the absorption at around 1400–2000 cm^{-1} bands. The BG-Te glass sample shows different behavior than the other samples, in which the intensity from about 550 to 1250 cm^{-1} is extremely intense than the other bands that indicate an increased generation

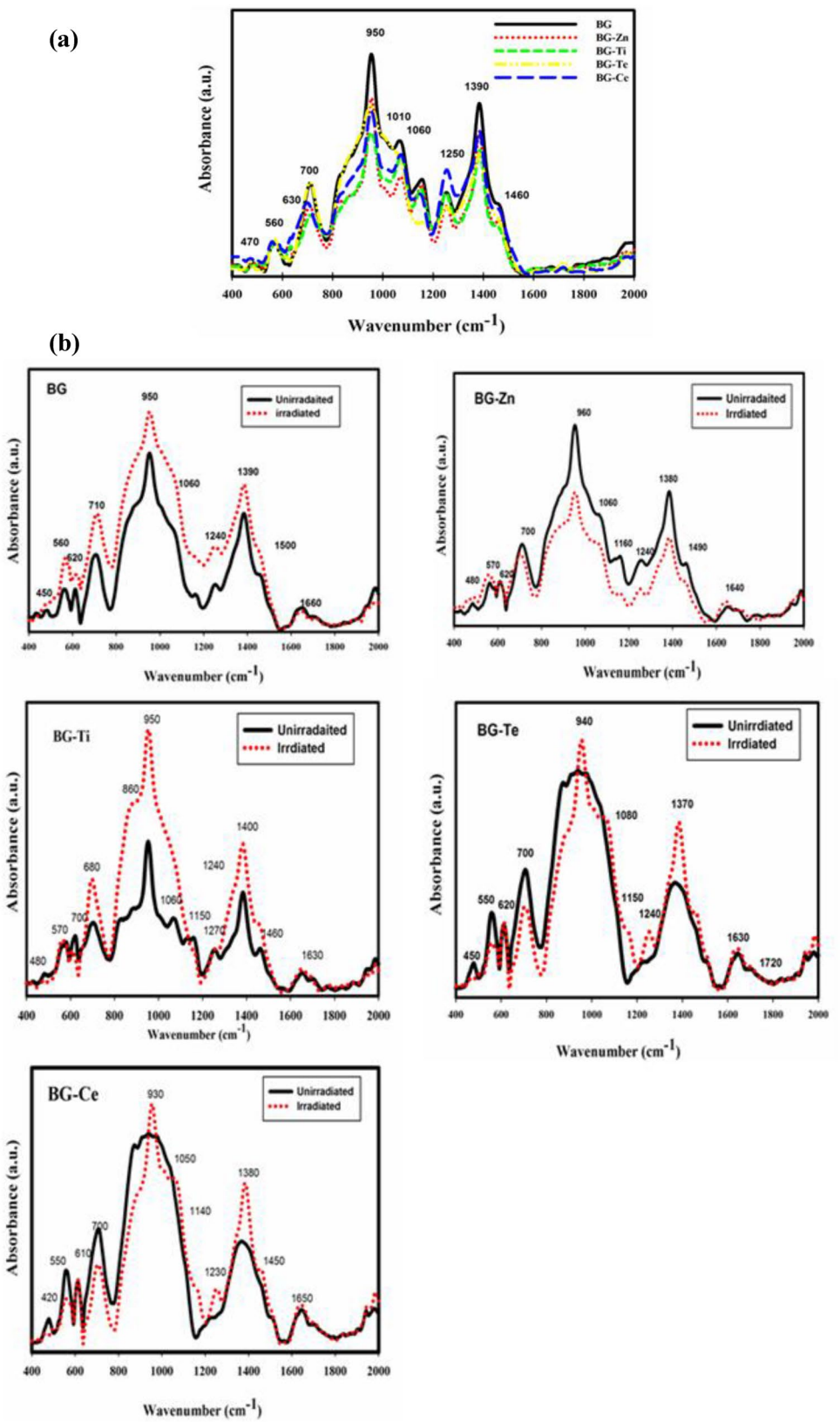

Fig. 2 **a** Infrared absorption spectra of un-doped and doped glasses with 2% of ZnO, TiO_2, and CeO_2. **b** Comparing the IR spectra of the samples before and after gamma irradiation after immersion in SBF

of BO_4 groups in the glass. However, the changes at around 1200–1500 cm^{-1} bands are not observed. This process requires additional studies through several techniques.

Interpretation of the FTIR spectra of investigated glass system after immersion

Figure 2b also, demonstrated the FTIR spectra of the prepared glass powder after soaking in SBF for two weeks, The ability of borate glasses to hydrolyze and create B–OH bonds when exposed to the solution is linked to the efficiency of B_2O_3 [11, 13]. The most important new features in all these spectral curves are the appearance of two IR peaks at about 510-560 and 680-720 cm^{-1} in all the studied samples. Some important changes identified in the spectra such as the detected variations in the intensities of several vibration bands were due to the difference in solubility of various mixed borate phases [30]. These newly formed peaks are associated with the production of the hydroxyapatite phase (calcium phosphate) which is a positive evidence of the glass bioactivity. Identification of a new band at bands about 510-560 and 680-720 confirms the formation of hydroxyapatite [31–33].

Interpretation the effect of gamma radiation on the FTIR spectra of investigated glass system after immersion

Gamma irradiation has been mostly presented as an efficient sterilization technique further, enhancement the characteristics of bulk materials, and modifying surface defects. The increase of glass dissolution by gamma irradiation is due to the generation of non-bridging oxygens throughout the glass network or breaking of bonds or differences in the bond angles, or radiolysis [34]. Primak [35] described that radiation causes the reduction the building units bond angles that explain the greater IR bands intensities. So, the observed peaks at 500–1600 cm^{-1} are formed by the effect of radiation as shown in Fig. 2b. In the light of the above discussion, it can demonstrate the FTIR spectra of irradiated glass samples after soaking in SBF for two weeks. As shown from the IR spectra, there are several main changes observed in the absorption band for BG, BG-Ti, BG-Te, and BG-Ce glasses, which are around 950 and 1390 cm^{-1}. The intensity of these absorption bands is seriously increased after irradiation, indicating the increase of the BO_3 group with non-bridging oxygen. On the other hand, the FTIR spectra after radiation for BG-Zn glasses show very small changes compared to before irradiation. This indicates that BG-Zn glasses are resistant to gamma radiation compared to other glasses.

In the earlier evidence to understand the IR spectra, it should be considered the theory of independent vibrations of various functional groups presented by Tarte [36] and Margha and Abdelghany [37]. Based on independent vibrations, it is important to get explanations of the concerned vibrational peaks to discover the probable hidden or overlapped peaks needed to identify the component peaks of the FTIR spectra to indicate their assignment.

As shown in Fig. 3. the bands in the deconvoluted spectra by Peak fit programme of the irradiated bioactive borate glasses were at 420, 850, 1040, 1160, 1310, 1460, and 1620 cm^{-1}. So, the sequence starts through the hydrolysis step of the glass surface, and the additives are found from the SBF solution and instead are replaced with hydronium and (B–OH) creation [38]. The first distinct peak is located around 850 cm^{-1} because the boron is the lightest glass-forming element. The band around 1040 cm^{-1}, can be assigned to vibrations of tetra-coordinated borate (BO_4) groups. The two bands 1160 and 1310 cm^{-1} (ascribable to PO_4 vibration. The two bands at 1460 and1620 cm^{-1} are related to vibrations of carbonate, water, and OH groups [39]. The (B–O alkali connections) vibrations were about 800–1200 cm^{-1}, showing a weakening in amplitude during immersion [40]. During the immersion process, the ion-exchange process was initiated. In the light of the results, the corrosion percent increased when glass was irradiated. Also, it realized that there is a minor shift in borate groups and their intensity decreases [41, 42].

Effect of glass composition on weight loss

When immersion the studied glasses in SBF for two weeks from Fig. 4 shows the weight loss data of studied glass samples increased with time. The weight loss percent data from the studied samples confirm the following variations, The solubility of glass depend on: the chemical composition of the glass, such as the concentration of triangle BO_3 and tetrahedral BO_4 groups in the glass system and also, the amount of the alkali and alkaline ions, which are lightly bound and may be easily detached thru leaching ion-exchange processes to the solution and on condition of immersion including temperature, and time [43]. So, it is accepted that dependable glass system displays a controlled ion-exchange reaction among the leaching solution (SBF) and the constituent alkali and alkaline ions from the studied glass system. It is recognized that nearly all sodium compounds are readily soluble and consequently, the released Na^+ ions from the studied glass are continuously replaced by protons (H^+) or hydronium ions $(H_3O)^+$ from contact solution fluid, but the Ca^{2+} and P^{5+} are much more slowly than H^+ or $(H_3O)^+$ than Na^+, blocking the pathway canals during the corrosion mechanism,when glass is dipping in an aqueous solution [44]. In the light of above discussion can be remarked that BG glass samples lower weight loss value than the other samples due to

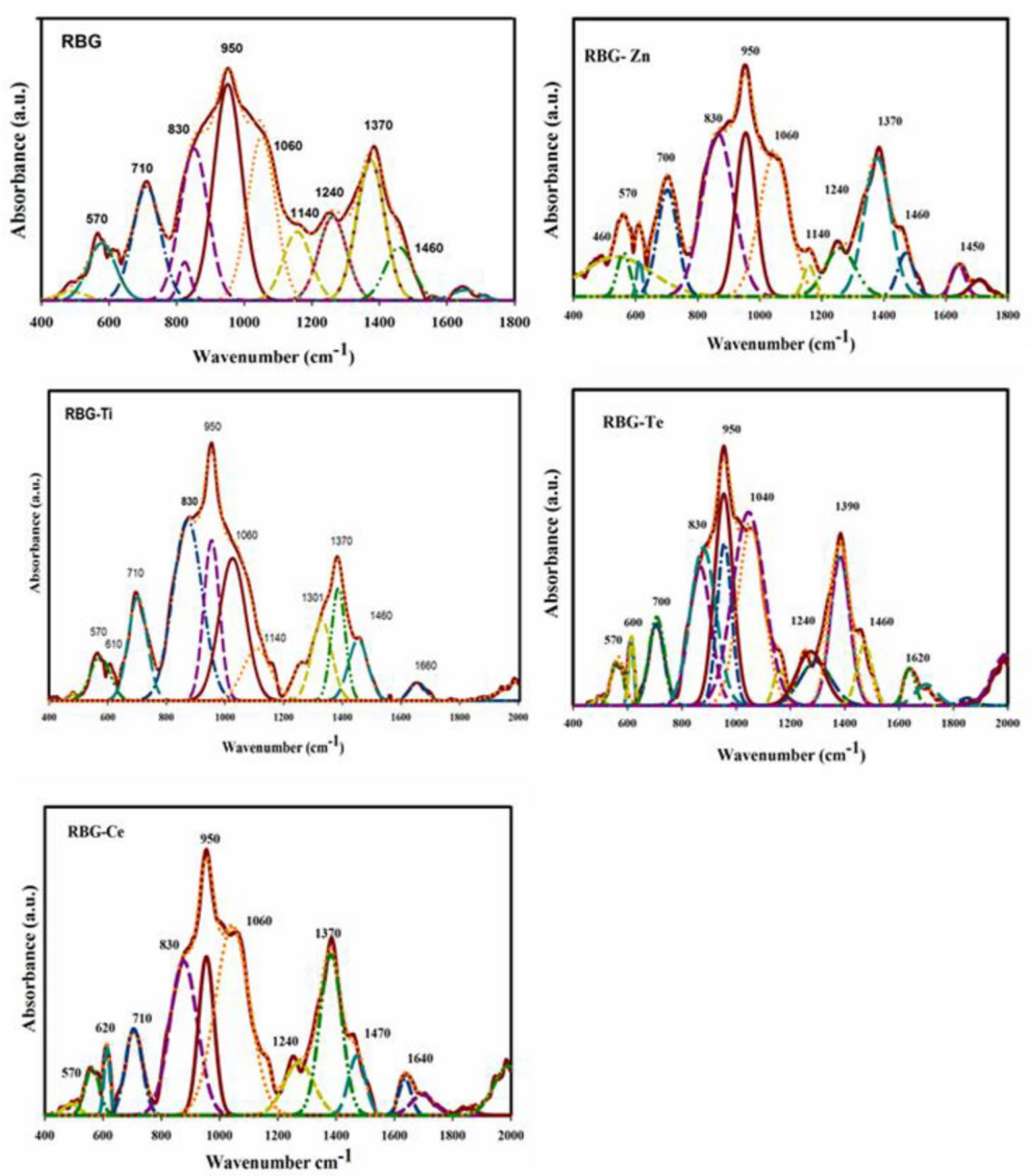

Fig. 3 Deconvoluted FT-infrared absorption spectra of irradiated glass system after immersion in SBF for 14 days

the presence of phosphorus which is responsible for the formation of the apatite layer (calcium phosphate), which is eventually deposited on the glass surface and retard the progress of corrosion. The various impacts of dopants are related to or based on their ability to create soluble species or ionic products [45]. However, BG-Zn and BG-Ti glass sample have higher weight loss value than base glass, this was likely due to presence of ZnO or TiO_2 or Te_2O_3 into the borate network as a modifier, it would create additional NBO that may be helpful in openness of the glass structure and thus increase the corrosion [46]. In another hand, the existence of weighty metal oxide such as TeO_2 modifies the structural arrangements in the glass causing some degree of disorder of the non-crystalline structure [46] BG-Ce glass sample was revealed higher weight loss than the other glass samples and so higher corrosion value. Similarly, CeO_2 was increased the number of (NBOs) and increased the reactivity of the surface which help of formation the apatite layer [47]. Although the specifics of their processes require more analysis.

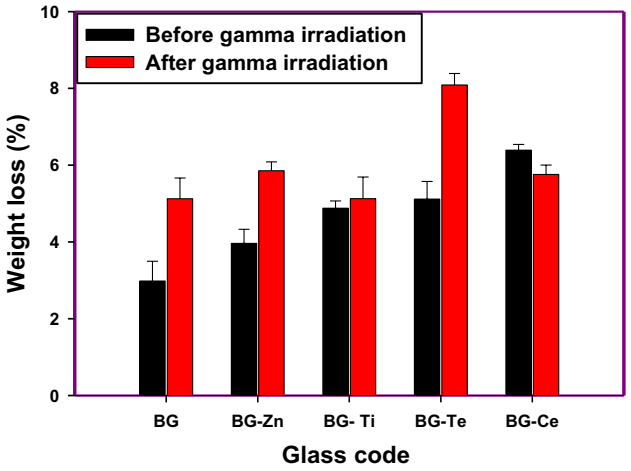

Fig.4 Weight loss of both glass and irradiated glass after immersion in SBF Solution 14 days

Effect of gamma irradiation on corrosion of prepared glasses

When immersion the irradiated glasses in SBF for two weeks as illustrated in the Fig. 4 the degradation rate of the borate glass samples increased. The degradation rate difference can be explained as the effect of irradiation on glasses may produce surface disrupt and immigration of non-network cations. These blemishes cause an acceleration of the leaching procedure, which may be resulted from the improvement of the breakthrough of protons or hydronium ions from solution to the glass structure [48]. The induced damage may be exemplified by the presence of big vacancies that took place after gamma irradiation. Nevertheless, a series of bond-breaking events could occur, causing large molecular islands to disintegrate from the glass surface. According to the latest facts, the glass system consists of collective blemishes from the borate and phosphate partners, as well as the possible sharing of the trace Tellurium ions. When the glass system was exposed to gamma irradiation it became ionized and exhibited numerous blemishes. However, the observed results in glass sample BG-Ce display enhancement of glass durability with irradiation that could be due to destruction of some blemishes or rebinding in the glass matrix [48, 49]. The authors of the present work accept this postulation and assume that further work is still needed to justify with contemporary techniques the actual state of the blemishes obtained from bioglass, specifically the sharing of all the borate and phosphate partners.

Scanning electron microscope (SEM)

Figure 5 represents SEM micrographs of; the glass samples after immersion for 14 days in SBF solution, bioactive borate glass, and gamma-irradiated samples. After comparing these micrographs, the creation of hydroxyl carbonated apatite (HCA) on the surface of bioactive glass was noticed. This creation of HCA considers as a guidance of bioactive

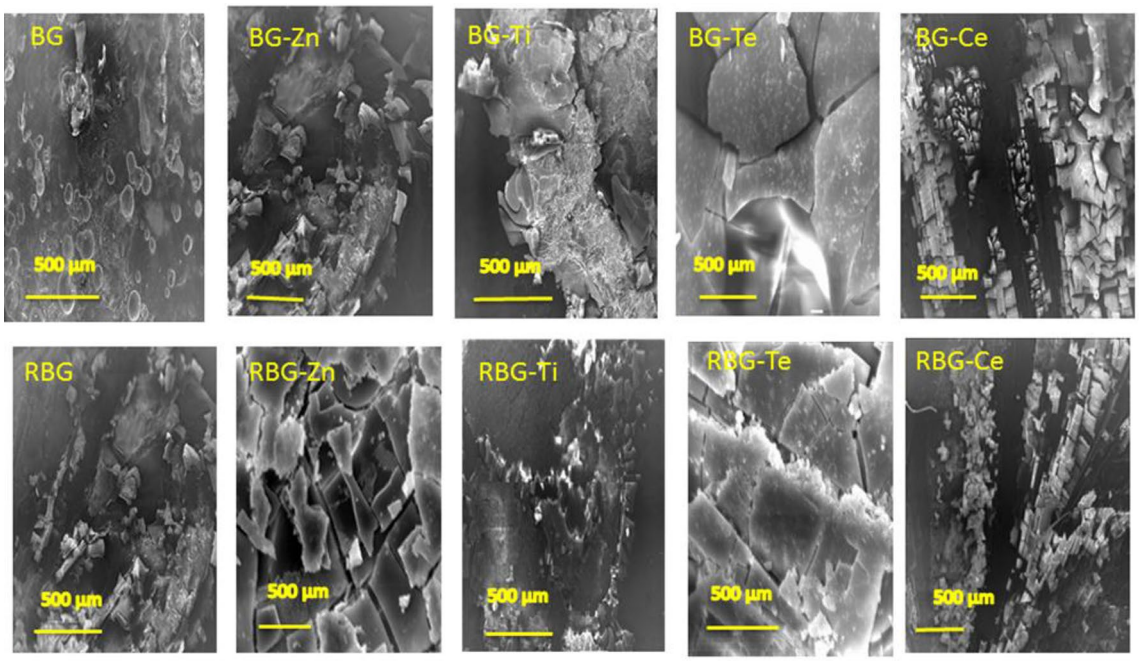

Fig. 5 SEM photographs of un-irrdiated and irradiated glasses after immersion in SBF for 14 days

borate glass characters. Interestingly, neither gamma irradiation nor MO addition altered the bioactivity of the glass system [50].

Agar well diffusion assay

Usually, antimicrobials are used to control microbial infections originating from clinical poisonings; the main example is *S. aureus* infection-causing osteomyelitis. Nevertheless, borate glass has newly obtained great attention as they are exclusively used to resist pathogenic microorganisms [51]. In the present study, borate glass was investigated for its antibacterial ability utilizing the well agar diffusion method. The borate glass samples used in the antibacterial test are (BG, BG-Zn, BG-Ti, BG-Te, and BG-Ce). Further, the borate glass was applied on *S. aureus* ATCC 6538 with concentrations of 10.0, 20.0, and 40.0 mg/mL after and before gamma irradiation at 25.0 kGy. As represented in Fig. 6, it was found that the concentrations of 20.0 and 40.0 mg/mL have high antibacterial effects rather than 10.0 mg/mL in both the irradiated and un-irradiated samples. The antibacterial activity of gamma-irradiated glass at 25.0 kGy has a slightly weaker effect on *S. aureus* ATCC 6538. As observed from the results in Fig. 6., the BG-Te at a concentration of 20.0 mg/mL shows a mean inhibition zone (ZOI) of 40.0 ± 1.020 mm for the un-irradiated sample and 35 ± 1.340 mm for the 25.0 kGy irradiated samples. With a concentration of 40.0 mg/mL, the un-irradiated sample records an inhibition zone of 35 ± 0.785 mm and 25 ± 0.780 for the gamma-irradiated samples. It was found from the results, the antibacterial activity of gamma-irradiated borate glass at 25.0 kGy has slightly less effect against *S. aureus* ATCC 6538. The BG-Ti at a concentration of 20.0 mg/mL shows (ZOI) of 20.0 ± 0.430 mm for the un-irradiated and 20.0 ± 0.730 mm for the irradiated samples (Fig. 6). Moreover, the (ZOI) of 40.0 mg/mL of BG-Ti is 22.5 ± 0.214 mm in the un-irradiated sample and 20.0 ± 0.014 mm in the irradiated sample. There is no antibacterial effect that can be detected for base borate glass samples. This could be explained as the amount of released boron is being extremely low to inhibit bacterial growth. Hence, the deposition of specific ions in the bioglass is advisable to perform high antimicrobial effects. BG-Zn and BG-Ce do not have an antibacterial effect. Despite, gamma irradiation does not have an improving effect on the antibacterial activity of borate bioglass but also does

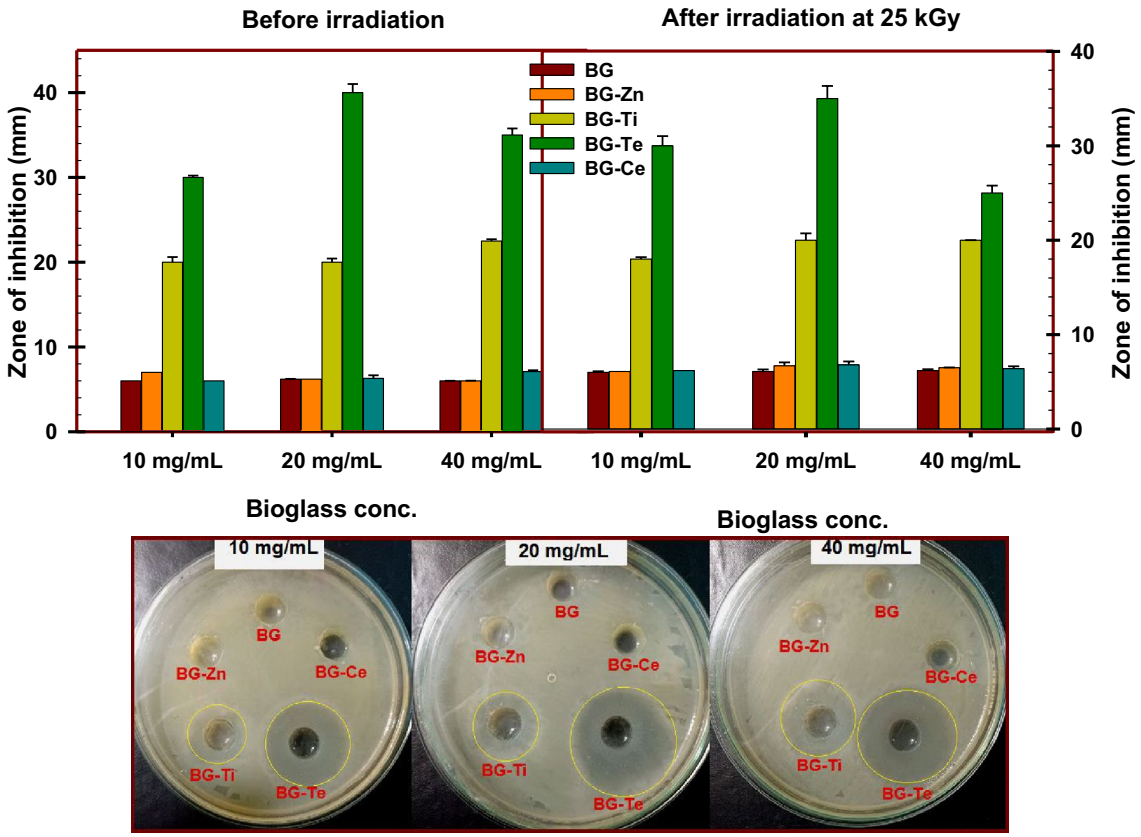

Fig. 6 The antibacterial activities of the borate bioglasses (BG, BG-Zn, BG-Ti, BG-Te, and BG-Ce) at concentrations of 10.0, 20.0, and 40.0 mg/mL after and before gamma irradiation at 25.0 kGy against *S. aureus* ATCC 6538. The error bar represents the standard error ($n = 3$)

not have a negative effect on the glass properties. So, it may be used for sterilization of glass to be used in medical applications. The antimicrobial potency is considerably depending on the particle size. The small particle size presented a potent influence as an antimicrobial mediator [29]. The increase in borate bioglass concentration over 20.0 mg/mL causes a partial aggregation of particles. This aggregation consequently results in an elevation in the particle size reducing the antimicrobial effect.

It was previously reported from the literature that in an aqueous medium the metal-doped glass gradually dissolves depending on its dissolution rate. During its dissolution, the ions incorporated into the bioglass construction are released into the medium. One of the mechanisms considered to be accountable for their antibacterial influences is the release of their ionic compounds over time [52–54]. *S. aureus* ATCC 6538 is a Gram-positive bacteria that principally have a thicker layer of peptidoglycan in their cell wall composition [55]. A further study reported that 45 mg/mL of F18 bioactive glass may inhibit the entire community of methicillin-resistant *S. aureus* (MRSA) [56].

The MIC dilutions from 3.125 to 25.0 mg/mL of BG-Ti and BG-Te against *S. aureus* ATCC 6538 were estimated. The MIC of the BG-Ti and BG-Te is 12.5 mg/mL. The characteristics of the BG-Te represent an important function in their antimicrobial activity, such as their structure, purity, and size. *S. aureus* may enter into the bloodstream through a skin injury. The *S. aureus* then transfers and targets the bone tissues causing severe inflammation called osteomyelitis. After treatment, Borate glass particles attack *S. aureus* resulting in intense damage to the bacterial cells ending with cells death as described in Fig. 7.

The basic object that explains the action mechanism of bioactive glasses in the removal of microbes in various studies is the raise of the pH that results in the development of osmotic pressure. Furthermore, needle-shaped glass can destroy the cell wall inducing bacterial death [57, 58]. Passos et al. [56] described a different way that could be affected the antibacterial potency of bioactive glass. When bacteria are joined to the bioactive glass, calcium liberates in a large amount in the closeness of the plasma membrane, and that change the electrochemical potential, ending cell death. Numerous literature explained the possible impacts of metals on the pathogenic microbes using advanced devices, like reactive oxygen species (ROS) distribution (superoxide anion; O^{2-}) [59]. Thus, the interaction of BG-Te with *S. aureus* causes the alkaline propensity that may be explained as the probable antimicrobial impact [47].

Borate bioglass has been attested to improve wounds healing where borate has antimicrobial potential mechanisms include energy reduction. This reduction is performed by binding to NAD and NADH of the microbes, connecting to ribose groups, and starting DNA destruction[2].

The antibiofilm activity of the BG-Te against *S. aureus* ATCC 6538

Biofilm production is recognized in numerous bacteria that produce exopolysaccharides [60]. Biofilm production by *S. aureus* ATCC 6538 was estimated by tube method. *S. aureus* was grown on a nutrient broth medium supplied with and without the BG-Te at concentrations of 10.0, 20.0, and 40.0 mg/mL. In the case of control sample (without BG-Te), a compact whitish-yellow matt of *S. aureus* was

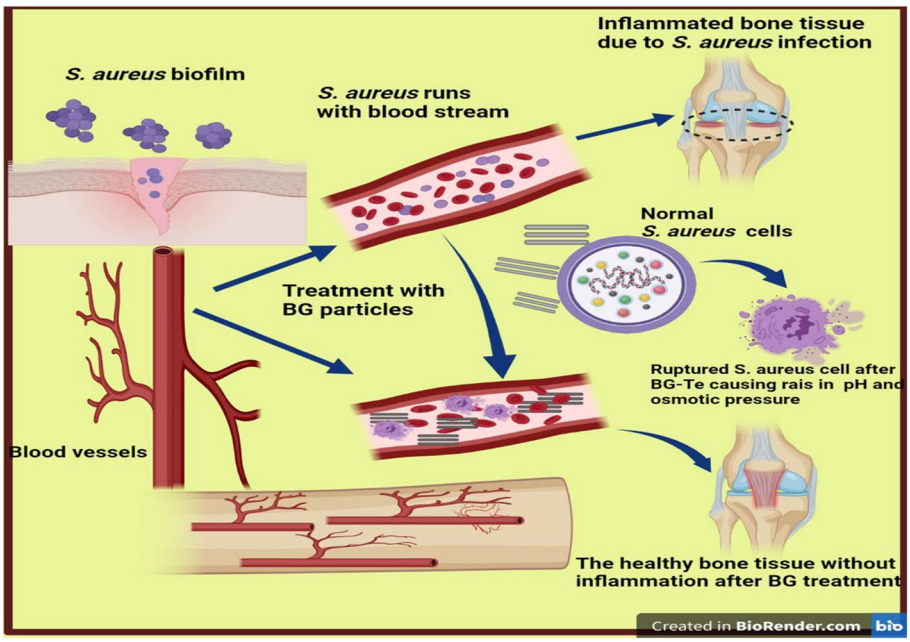

Fig. 7 The infection of bone tissue by *S. aureus* resulting in osteomyelitis and treatment with borate bioglass. The borate bioglass cause rupturing of *S. aureus* cells and maintaining healthy normal bone tissue

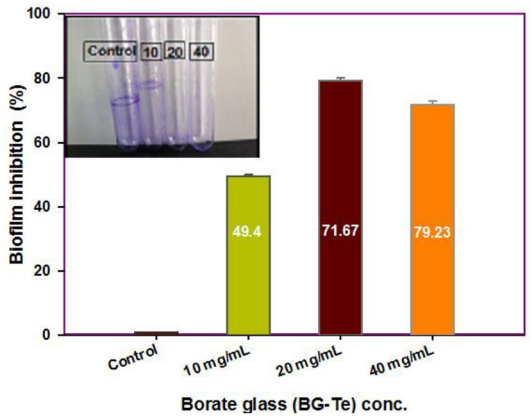

Fig. 8 The antibiofilm activity of BG-Teat concentrations of 10.0, 20.0, and 40.0 mg/mL against *S. aureus* ATCC 6538 by test tube method showing the highest percentage of biofilm reduction at 20.0 mg/mL

created on the medium surface adhered to the tube walls. On the other hand, the BG-Te at concentrations of 10.0, 20.0, and 40.0 mg/mL hinder bacterial growth ring development. After staining by crystal violet dye and further dissolving using ethanol, the control tubes show deep blue solution while the treated tubes show a faint blue color that reflects the biofilm inhibition activity of BG-Te as shown in Fig. 8. The blue color intensity was evaluated using UV–Visible spectrophotometer at $\lambda = 570.0$ nm. The BG-Te concentration of 20.0 mg/mL displays the maximum biofilm inhibition percentage (79.23%) while 10.0 mg/mL concentration represents the lowest as shown in Fig. 8. Various mechanisms described how the biofilms synthesized on the surfaces, as the genes responsible for the adhesion and the generation of the extracellular polysaccharides. The exopolysaccharides promote bacterial growth in the biofilm to protect themselves from the antibacterial factors in the environment and the host resistance [22]. So, the *S. aureus* ATCC 6538 incubated without BG-Te treatment shows a cloudy yellowish matt, indicating the production of exopolysaccharides that are required for the progress of biofilm (Fig. 8). While the *S. aureus* that inserted with BG-Te is inhibited. Therefore, if the exopolysaccharide production is reduced, the bacteria cannot synthesis the biofilm. Lastly, to eradicate biofilms, the antibacterials should enter the polysaccharide film to destroy the bacterial cells [61].

The comparative study of Coraça-Huber et al. [62] indicated that BG- S53P4 has the potency to be used in joint replacement surgeries as a bone substitute and cure chronic osteomyelitis. Bioactive glass S53P4 can inhibit the biofilm formation of *S. aureus*. Also, F18 bioactive glass exhibited bactericidal potency against *S. aureus* and MRSA biofilms, suppressing over 6 times of the viable cells that were treated with 50 mg/mL for 24 h[56]. Tellurium (Te) has sparked attention as possible antibacterials in current years. Tellurium was shown to have antibacterial and biofilm eradication action against *S. aureus* [63]. Te particles can pass the cell membrane of bacteria and produce injury to cellular elements through generating reactive oxygen species. These changes inhibit the enzymes activity and DNA assembly while also affecting energy transfer [64]. Te ions filtrated from the bacterial solution can be reduced to elemental Te^0 by some bacteria, resulting in nanoparticles formation. A flavine-dependent reductase in the plasma membrane is hypothesized to be accountable for the reduction of the ions [16].

Kinetics of *S. aureus* ATCC 6538 growth

The effect of BG-Te on *S. aureus* ATCC 6538 growth was analyzed. As revealed in Fig. 9, the growth rate of *S. aureus* ATCC 6538 of the control sample occurs rapidly. The optical density of control at $\lambda = 600$ nm (OD_{600}) is 1.52 nm. In contrast, the OD_{600} values of BG-Te are lower than control that is because of the superior antibacterial activity of borate glass. The rate of growth inhibition of *S. aureus* ATCC 6538 as a result of BG-Te treatment is significantly starting from the first time of observation until the endpoint of 24 h. There is no difference between the effect of 20.0 and 40.0 mg/mL concentrations at the first 8.0 min of observation after that 20.0 mg/mL exerts an additional suppressing effect more than 40.0 mg/mL that proved by the optical density readings (Fig. 9). The results can be explained as the growth rate of *S. aureus* within the concentration of 40.0 mg/mL is more than the growth in the presence of 20.0 mg/mL. To an antimicrobial drug can destroy an organism, it must attach to its target sites on the bacterial cells also must occupy a specific number of binding sites, which is correlated to its concentration within the microorganism. To contact with the binding

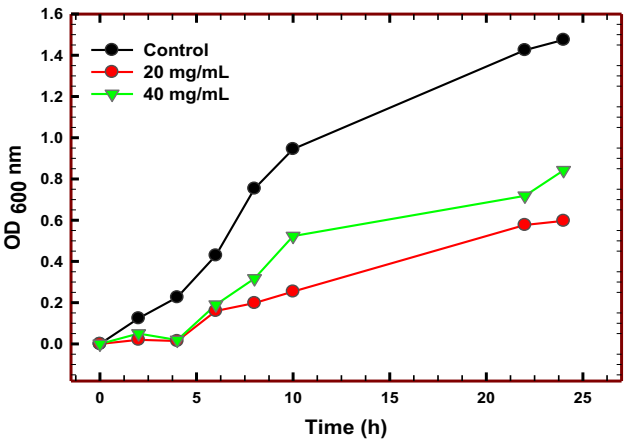

Fig. 9 Effect of BG-Te at concentrations of 20.0 and 40.0 mg/mL on thekinetics of *S. aureus* ATCC 6538 growth with time intervals (h)

sites, it must permeate through the outer membrane of the organism, avoid being pumped out (efflux pump resistance), and continue intact as a molecule (e.g., avoid hydrolysis by beta-lactamases). The antimicrobial can still be ineffective if the binding site has shifted its molecular configuration and no longer permits the antimicrobial drug to attach. Thus, by binding the drug to these sites, it conflicts with the chemical reaction causing the bacterium death. In some times the high concentration of the antimicrobial drug may cause an excess in the adequate number of binding sites that resulting in an interruption in the penetration rate of the drug [65]

The four main action mechanisms of the majority of antibacterial agents are inhibition of; protein synthesis, RNA and DNA synthesis, metabolic pathway [66]. As well, Zare et al. [67] reported that tellurium nanoparticles showed antibacterial potency against *K. pneumonia*, *S. aureus*, and, *S. typhi*, at 125, 500 mg/L.

Hu et al. [68] showed that 45S5 bioglass presented an effective antibacterial impact towards a large variety of bacterial strains. The probable mechanisms of the antibacterial impact of bioactive glass may be due to the presence of bioglass debris on the bacteria cell. Also, the greatest diameter of inhibition zone in borate glasses samples has been observed with *S. aureus* [69, 70].

Viable cell counts of *S. aureus* ATCC 6538

Viable cell number reduction of *S. aureus* ATCC 6538 represented as $\log_{10}$ CFU/mL, after overnight exposure to concentrations of BG-Te, 20.0 and 40.0 mg/mL. The results show the efficient microbial inhibition activity of BG-Te (20.0 and 40.0 mg/mL) against *S. aureus* ATCC 6538 comparable to the control. Bacterial inhibition has been estimated within the range from 10^{-4} to 10^{-6} serial dilutions of the *S. aureus* inoculum. As shown in Fig. 10, BG-Te starts reducing the number of colony-forming units of *S. aureus* after the 10^{-3} dilution while complete inhibition occurs at the 10^{-4} and 10^{-5} dilutions in case of 20.0 and 40.0 mg/mL, respectively. In contrast, the bacterial growth of the control sample (without BG-Te) shows a high number of colony-forming units even at the 10^{-5} dilution. As predictable, the values of $\log_{10}$ confirm the results obtained from the viable cell count assay where 20.0 and 40.0 mg/mL recorded $\log_{10}$ (4.477 and 6.477) compared to $\log_{10}$ of the control (7.041).

In a similar study by El-Tablawy [19] where the colony-forming units of all MRSA, *E. coli,* and *P. aeruginosa* decreased by one log cycle, according to the treatment with bioglass 45S5. Naseri et al. [54] found that the borate-based glasses displayed a notably higher antibacterial behavior that the silica-based glasses with 15 mol% of TiO_2 included exceeding the other tested glasses. The titanium addition to borate bioglass composition is desirable to reduce the bacterial growth on the surface of borate bioglass [71]. Another study by Boschetto et al. [72] examined the efficiency of chitosan/polyethylene oxide-bioactive glass with titanium against *S. epidermidis* and SaOS-2 human osteosarcoma cell line. The viability and colony-forming unit count assay revealed a significant reduction in bacterial growth after treatment. Chitosan/polyethylene oxide-bioactive glass with titanium could enhance the antibacterial and osteoconductive features and could be used as a strong applicant for orthopedic treatments. Cunha et al. [73] tested the growth inhibition efficiency of borate bioglass against *S. aureus* for 120 h incubation time. Borate bioglass approached zero CFU/mL among 120 and 168 h and exhibited a reduction of about 1 $\log_{10}$ every 24 h.

Protein content of *S. aureus* ATCC 6538

The protein contents of *S. aureus* ATCC 6538 biofilm were estimated using Bradford Coomassie brilliant blue test. The protein contents were determined for *S. aureus* supernatants that were treated with BG-Te concentrations of 0, 20.0, and 40.0 mg/mL. The experiments were assessed in triplicate, and the total protein contents are displayed in Fig. 11. At 20.0 and 40.0 mg/mL of BG-Te, the protein concentrations of *S. aureus* supernatants record (90.87 and 69.2 µg/mL, respectively) which is significantly lower than the untreated control (269.34 µg/mL).

A probable explanation for the variation in protein content may be correlated to the complicated metabolic processes of the bacterial cells as growth, reproduction, and biofilm formation. During the bacterial metabolic processes (macromolecule polymers, the cytotoxic substances, and metabolites, and bacterial lysis), some substances are liberated in high amounts. These substance are proteins, polysaccharides, lipids, and phospholipids [74].

Bradford Coomassie brilliant blue G-250 dye is available in a number of three patterns: firstly the cationic pattern, then neutral, and finally the anionic pattern. Though the anion does not exist in the free form at the dye reagent pH, this form can be combined with protein. Macromolecules with specific reactive functional groups are needed to bind with the dye. Cooperations are particularly with arginine that occurred by the electrostatic attraction, making a complex, efficient dying of proteins preferably than main amino groups. While, the basic (Histidine, Lysine) and aromatic (Tryptophan, Tyrosine, and Phenylalanine) groups provide inadequate interaction. The stain mechanism of the binding is revealed to hydrophobic connections and Van der Waals forces analysis intervention by different substances are described by their impacts upon the balance between the three dye patterns [75].

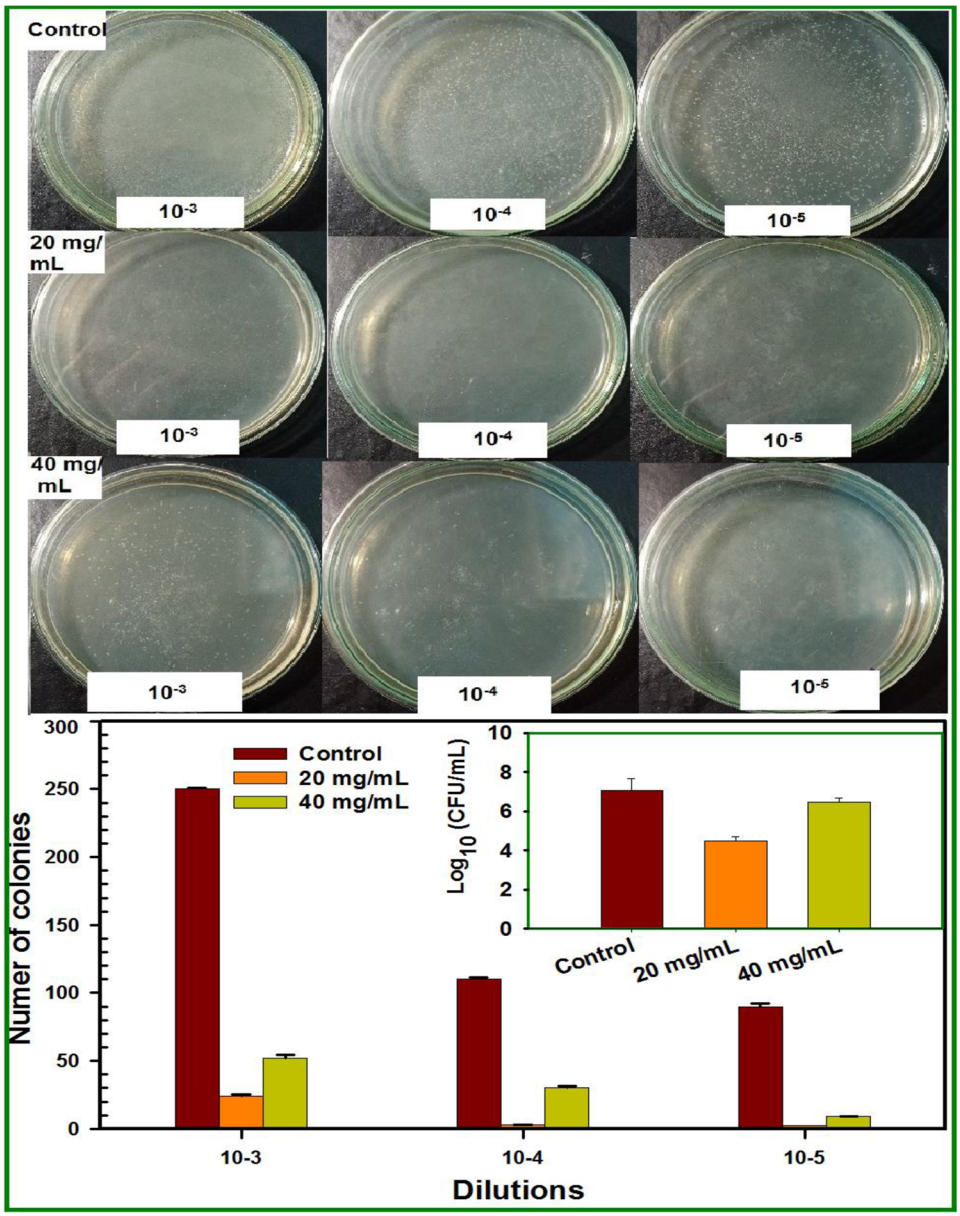

Fig. 10 Effect of BG-Te at concentrations of 20.0 and 40.0 mg/mL on the viability (number of colonies and $\log_{10}$) of *S. aureus* ATCC 6538

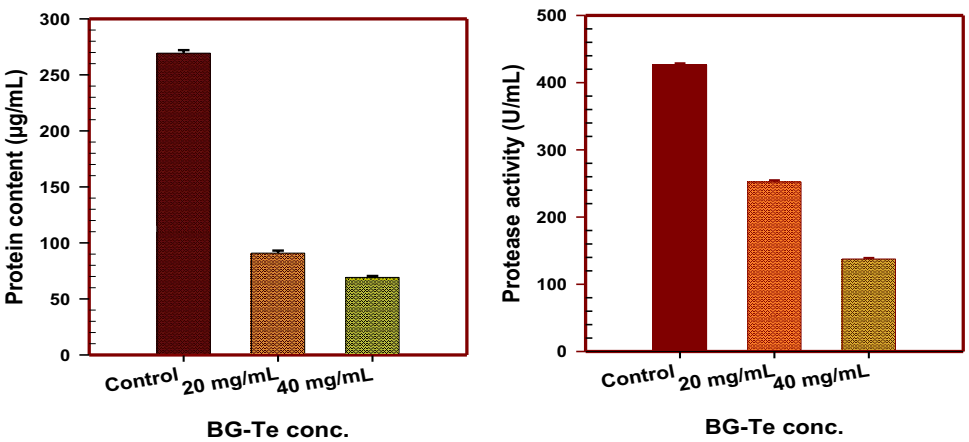

Fig. 11 Effect of BG-Te at concentrations of 20.0 and 40.0 mg/mL on the protein content and protease activity of *S. aureus* ATCC 6538

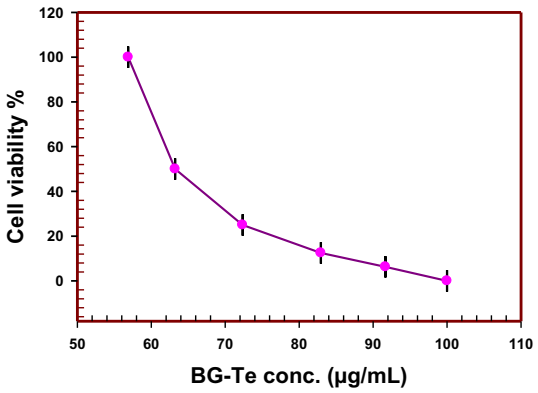

Fig. 12 Effect of BG-Te at concentrations of 20.0 and 40.0 mg/mL on the cell viability % of human fibroblast cells (WI-38)

Protease activity assay of *S. aureus* ATCC 6538

The synthesized BG-Te was incubated with *S. aureus* ATCC 6538 culture cells developed to stationary phase. The results illustrate that *S. aureus* shows value of 137.51 U/mL of protease activity with BG-Teat 40.0 mg/mL compared to the untreated control culture (426.27 U/mL) as shown in Fig. 12. While 20.0 mg/mL of BG-Te shows 252.1 U/mL of protease activity. This lends credence to the theory that ions in the borate bioactive glass interact with the catalytic active site or induce a change in the enzyme, leading to decreased activity [76].

Proteases are group of enzymes that can degrade or cleave vulnerable substrates found in host tissues and immune cells. Metalloproteases, serine proteases, and cysteine proteases are among the proteases produced by *S. aureus*. Staphopain B (SspB), staphopain A (ScpA), aureolysin, and V8 protease are examples of specialized proteases. Staphopains have the ability to suppress the immune system and kill tissues. Aureolysin and V8 protease are likewise immune-evading enzymes [77].

Appraisal of the cytotoxicity of BG-Te

Figure 12 displays the effect of BG-Te on the human fibroblast cells (WI-38) proliferation by MTT assay. The cell viability % decreased considerably with increasing the borate glass concentration. The experiment was carried out with 100, 50, 25, 12.5, 6.25, and 0.0 µg/mL dilutions of BG-Te. The cytotoxic effect was detected from the first dilution of 6.25 µg/mL. It has been shown that as the bioactive glass concentration increases, the cell viability percent or WI-38 cells count in the MTT assay reduces.

The BG-Te shows a low cytotoxic effect on the human fibroblast cells and the MIC concentration is 130.0 µg/mL. So, borate bioglass could be used for the treatment of *S. aureus* bacterial infection especially those causing osteomyelitis with a low harmful effect on the human cells. This was compatible with Modglin et al. [78] who discussed that borate ion liberation may be alleviated in an medium related to the human serum containing microvasculature. At this point, it was explained that in spite of the toxicity, composites containing boron may authorize for application in tissue engineering.

In similar results Rismanchian et al. [79] confirmed that two bioactive glasses had a considerable cytotoxicity on human gingival fibroblast cells at 5.0, 10.0, 15.0, and 20.0 mg/mL concentrations. In the normal human fibroblast cells, the MTT assay found no substantial cytotoxicity of magnesium doped bioactive glass, while in vivo tissue histology confirmed no noticeable harm to the cells [80]. Shoaib et al. [81] also found no tissue injure, excellent biomedical qualities, and no interference with the cell cycle of the potassium doped bioglass (even at a dose of 80 g/mL) in the animals studied and cytotoxicity investigations. Furthermore, at 20.0 µg/mL, cell proliferation assay showed that MBG is non-toxic.

Conclusion

In vitro bioactivity behavior of borate glass system doped with ZnO, TiO_2, TeO_2, or CeO_2 has been characterized and investigated. X-ray diffraction analysis was performed to recognize the amorphous phases of samples. Structural FTIR spectra indicate prominent characteristic vibrational bands due to BO_3 and BO_4 groups in their wavenumbers. After immersion for two weeks in SBF solution which supports bioactivity behavior, it is observed to generate two peaks concerned with hydroxyapatite (calcium phosphate). Weight loss data show that irradiated glass was noticeably corroded than un-irradiated. SEM micrographs of glass and irradiated glass before and after soaking in SBF solution reveal the formation of some nodular or rounded microcrystalline phases. Borate glasses dropped with metals were analyzed for their antibacterial potency against methicillin-resistant *Staphylococcus aureus* (MRSA) ATCC 6538. It was found that BG-Te displayed the maximum antibacterial effect. BG-Te significantly reduced the biofilm produced by *S. aureus*. A remarkable decrease in the number count, viability, and biochemical characteristics of the bacterial cells was observed. Also, studying the cytotoxicity of BG-Te on human fibroblast cells (WI-38) was a crucial parameter to be considered where it has low cytotoxicity on human cells. Finally, borate bioglass could be a potential candidate for antibacterial and bone repair tissue engineering applications.

Author contributions All authors were contribute in the output and writing the manuscript. Dr.W.M. Abd-Allah has synthesized and

characterized the borate bioglass and analyzed the results. Dr. Rasha Mohammad Fathy accomplished the antibacterial and cytotoxicity experiments and analyzed the results.

Funding There was no funding provided.

Availability of data and material The data are clearly applicable and the materials used are available.

Declarations

Conflict of interest The authors declare that they have no conflict of interest.

Informed consent to participate Not Applicable.

Ethical approval No humans or animal experiments were included in the study therefore, no ethical approval was acquired.

References

1. Reddy J (2006) Mechanics of advanced materials and structures. Mech Adv Mater Struct 13:443–455
2. Ottomeyer M, Mohammadkah A, Day D, Westenberg D (2016) Broad-spectrum antibacterial characteristics of four novel borate-based bioactive glasses. Adv Microbiol 6(10):776–787
3. Maany DA, Alrashidy ZM, Ghany NAA, Abdel-Fattah WI (2019) Comparative antibacterial study between bioactive glasses and vancomycin hydrochloride against *Staphylococcus aureus*, *Escherichia coli*, and *Pseudomonas aeruginosa*. Egypt Pharm J 18(4):304
4. Liang W, Rahaman MN, Day DE, Marion NW, Riley GC, Mao JJ (2008) Bioactive borate glass scaffold for bone tissue engineering. J Non-Cryst Solids 354(15–16):1690–1696
5. ElBatal FH, ElKheshen A (2008) Preparation and characterization of some substituted bioglasses and their ceramic derivatives from the system SiO2–Na2O–CaO–P2O5 and effect of gamma irradiation. Mater Chem Phys 110(2–3):352–362
6. Haque M, Sartelli M, McKimm J, Bakar MA (2018) Health care-associated infections–an overview. Infect Drug Resist 11:2321
7. Khaledi A, Weimann A, Schniederjans M, Asgari E, Kuo TH, Oliver A, Cabot G, Kola A, Gastmeier P, Hogardt M (2020) Predicting antimicrobial resistance in *Pseudomonas aeruginosa* with machine learning-enabled molecular diagnostics. EMBO Mol Med 12(3):e10264
8. Brown ED, Wright GD (2016) Antibacterial drug discovery in the resistance era. Nature 529(7586):336–343
9. Drago L, Toscano M, Bottagisio M (2018) Recent evidence on bioactive glass antimicrobial and antibiofilm activity: a mini-review. Materials 11(2):326
10. El-Batal H, ElKheshen AA, El-Bassyouni GT, Abd El Aty AA (2018) In vitro bioactivity behavior of some borate glasses and their glass-ceramic derivatives containing Zn^{2+}, Ag^{+} or Cu^{2+} by immersion in phosphate solution and their anti-microbial activity fatma. Silicon 10:943–957
11. Moghanian A, Ghorbanoghli A, Kazem-Rostami M, Pazhouheshgar A, Salari E, Saghafi Yazdi M, Alimardani T, Jahani H, Sharifian Jazi F, Tahriri M (2020) Novel antibacterial Cu/Mg-substituted 58S-bioglass: synthesis, characterization and investigation of in vitro bioactivity. Int J Appl Glas Sci 11(4):685–698
12. Karau MJ, Schmidt-Malan SM, Albano M, Mandrekar JN, Rivera CG, Osmon DR, Oravec CP, Berry DJ, Abdel MP, Patel R (2020) Novel use of rifabutin and rifapentine to treat methicillin-resistant *Staphylococcus aureus* in a rat model of foreign body osteomyelitis. J Infect Dis 222(9):1498–1504
13. Phetnin R, Rattanachan ST (2015) Preparation and antibacterial property on silver incorporated mesoporous bioactive glass microspheres. J Sol-Gel Sci Technol 75(2):279–290
14. Chien C-S, Lin C-J, Ko C-J, Tseng S-P, Shih C-J (2018) Antibacterial activity of silver nanoparticles (AgNP) confined to mesostructured silica against methicillin-resistant *Staphylococcus aureus* (MRSA). J Alloy Compd 747:1–7
15. Impey RE, Hawkins DA, Sutton JM, Soares da Costa TP (2020) Overcoming intrinsic and acquired resistance mechanisms associated with the cell wall of Gram-negative bacteria. Antibiotics 9(9):623
16. Matharu RK, Charani Z, Ciric L, Illangakoon UE, Edirisinghe M (2018) Antimicrobial activity of tellurium-loaded polymeric fiber meshes. J Appl Polym Sci 135(25):46368
17. Lu M, Liao J, Dong J, Wu J, Qiu H, Zhou X, Li J, Jiang D, He T-C, Quan Z (2016) An effective treatment of experimental osteomyelitis using the antimicrobial titanium/silver-containing nHP66 (nano-hydroxyapatite/polyamide-66) nanoscaffold biomaterials. Sci Rep 6(1):1–14
18. De Giglio R, Di Vieste G, Mondello T, Balduzzi G, Masserini B, Formenti I, Lodigiani S, Pallavicini D, Pintaudi B, Mazzone A (2021) Efficacy and safety of bioactive glass S53P4 as a treatment for diabetic foot osteomyelitis. J Foot Ankle Surg 60(2):292–296
19. El-Tablawy S, Abd-Allah W, Araby E (2018) Efficacy of irradiated bioactive glass 45S5 on attenuation of microbial growth and eradication of biofilm from AISI 316 L discs: In-vitro study. SILICON 10(3):931–942
20. da Silva Aquino KA (2012) Sterilization by gamma irradiation. Gamma Radiat 9:172–202
21. Baskaran C, Velu S, Kumaran K (2012) The efficacy of *Carica papaya* leaf extract on some bacterial and a fungal strain by well diffusion method. Asian Pac J Trop Dis 2:S658–S662
22. Fathy RM, Salem MSE-D, Mahfouz AY (2020) Biogenic synthesis of silver nanoparticles using *Gliocladium deliquescens* and their application as household sponge disinfectant. Biol Trace Elem Res 196(2):662–678
23. Salem MSE-D, Mahfouz AY, Fathy RM (2021) The antibacterial and antihemolytic activities assessment of zinc oxide nanoparticles synthesized using plant extracts and gamma irradiation against the uro-pathogenic multidrug resistant Proteus vulgaris. Biometals 34(1):175–196
24. El-Shazly AN, El-Sayyad GS, Hegazy AH, Hamza MA, Fathy RM, El Shenawy E, Allam NK (2021) Superior visible light antimicrobial performance of facet engineered cobalt doped TiO_2 mesocrystals in pathogenic bacterium and fungi. Sci Rep 11(1):1–14
25. Huang W, Wang J-Q, Song H-Y, Zhang Q, Liu G-F (2017) Chemical analysis and in vitro antimicrobial effects and mechanism of action of *Trachyspermum copticum* essential oil against *Escherichia coli*. Asian Pac J Trop Med 10(7):663–669
26. Kung J-C, Wang W-H, Lee C-L, Hsieh H-C, Shih C-J (2020) Antibacterial activity of silver nanoparticles (AgNP) confined to mesostructured, silica-based calcium phosphate against methicillin-resistant *Staphylococcus aureus* (MRSA). Nanomaterials 10(7):1264
27. Kiersztyn B, Siuda W, Chrost R (2017) Coomassie blue G250 for visualization of active bacteria from lake environment and culture. Pol J Microbiol 66(3):365–373
28. Arvidson S, Holme T, Lindholm B (1973) Studies on extracellular proteolytic enzymes from *Staphylococcus aureus*: I. Purification and characterization of one neutral and one alkaline protease. Biochim Biophys Acta BBA-Enzymol 302(1):135–148

29. Fathy RM, Mahfouz AY (2021) Eco-friendly graphene oxide-based magnesium oxide nanocomposite synthesis using fungal fermented by-products and gamma rays for outstanding antimicrobial, antioxidant, and anticancer activities. J Nanostruct Chem 11(2):301–321
30. Wu T, Li M, Zhu X, Lu X (2021) Research on non-pneumatic tire with gradient anti-tetrachiral structures. Mech Adv Mater Struct 28:2351–2359
31. Marzouk M, ElBatal F, Ghoneim N (2018) In vitro bioactivity behavior of modified multicomponent borate glasses containing dopants of Ag_2O, CuO, CeO_2 or V_2O_5. Appl Phys A 124(2):1–12
32. El Batal H, Azooz M, Ibrahim MM, Ali AM, Somaily H, Sayed M (2020) Bioactivity behavior of multicomponent (P_2O_5–B_2O_3-SiO_2-Na_2O-CaF_2) glasses doped with ZnO, CuO or Ag_2O and their glass-ceramics. SILICON 13:1–11
33. Thian E, Huang J, Vickers M, Best S, Barber Z, Bonfield W (2006) Silicon-substituted hydroxyapatite (SiHA): a novel calcium phosphate coating for biomedical applications. J Mater Sci 41(3):709–717
34. Luzhetsky AV, Petrov VA, Yudintsev SV, Malkovsky VI, Ojovan MI, Nickolsky MS, Shiryaev AA, Danilov SS, Ostashkina EE (2020) Effect of gamma irradiation on structural features and dissolution of nuclear waste Na–Al–P glasses in water. Sustainability 12(10):4137
35. Primak W (1972) Mechanism for the radiation compaction of vitreous silica. J Appl Phys 43(6):2745–2754
36. Tarte P (1964) Identification of Li-O bands in the infra-red spectra of simple lithium compounds containing LiO4 tetrahedra. Spectrochim Acta 20(2):238–240
37. Margha FH, Abdelghany AM (2012) Bone bonding ability of some borate bio-glasses and their corresponding glass-ceramic derivatives. Process Appl Ceram 6(4):183–192
38. Vallet-Regí M, Romero E, Ragel C, LeGeros R (1999) XRD, SEM-EDS, and FTIR studies of in vitro growth of an apatite-like layer on sol-gel glasses. J Biomed Mater Res 44(4):416–421
39. Kamitsos E (2003) Infrared studies of borate glasses. Phys Chem Glasses 44(2):79–87
40. Luo J, Smith NJ, Pantano CG, Kim SH (2018) Complex refractive index of silica, silicate, borosilicate, and boroaluminosilicate glasses–Analysis of glass network vibration modes with specular-reflection IR spectroscopy. J Non-Cryst Solids 494:94–103
41. Saudi H, Abd-Allah W (2021) Structural, physical and radiation attenuation properties of tungsten doped zinc borate glasses. J Alloys Compd 860:158225
42. Abd-Allah W, Saudi H, Shaaban KS, Farroh H (2019) Investigation of structural and radiation shielding properties of 40B2O3–30PbO–(30-x) BaO-x ZnO glass system. Appl Phys A Mater Sci Process 125 (4)
43. Rajendran V, Devi AG, Azooz M, El-Batal F (2007) Physicochemical studies of phosphate based P2O5–Na2O–CaO–TiO2 glasses for biomedical applications. J Non-Cryst Solids 353(1):77–84
44. Sharma K, Dixit A , Singh S, Jagannath, Bhattacharya S, Sharma PK, Yusuf SM, Tyagid AK, Kothiyala GP (2009) Preparation and studies on surface modifications of calcium-silico-phosphate ferrimagnetic glass-ceramics in simulated body fluid. Mater Sci Eng C 31(7):2226–2233
45. Koohkan R, Hooshmand T, Mohebbi-Kalhori D, Tahriri M, Marefati MT (2018) Synthesis, characterization, and in vitro biological evaluation of copper-containing magnetic bioactive glasses for hyperthermia in bone defect treatment. ACS Biomater Sci Eng 4(5):1797–1811
46. Brauer DS, Karpukhina N, Law RV, Hill RG (2010) Effect of TiO2 addition on structure, solubility and crystallisation of phosphate invert glasses for biomedical applications. J Non-Cryst Solids 356(44–49):2626–2633
47. Farag MM, Al-Rashidy ZM, Ahmed MM (2019) In vitro drug release behavior of Ce-doped nano-bioactive glass carriers under oxidative stress. J Mater Sci - Mater Med 30(2):18
48. Farag M, Abd-Allah W, Ahmed HY (2017) Study of the dual effect of gamma irradiation and strontium substitution on bioactivity, cytotoxicity, and antimicrobial properties of 45S5 bioglass. J Biomed Mater Res, Part A 105(6):1646–1655
49. Farag M, Abd-Allah W, Ibrahim A (2015) Effect of gamma irradiation on drug releasing from nano-bioactive glass. Drug Deliv Transl Res 5(1):63–73
50. Beherei HH, Mohamed KR, El-Bassyouni GT (2009) Fabrication and characterization of bioactive glass (45S5)/titania biocomposites. Ceram Int 35(5):1991–1997
51. Jia W-T, Fu Q, Huang W-H, Zhang C-Q, Rahaman MN (2015) Comparison of borate bioactive glass and calcium sulfate as implants for the local delivery of teicoplanin in the treatment of methicillin-resistant *Staphylococcus aureus*-induced osteomyelitis in a rabbit model. Antimicrob Agents Chemother 59(12):7571–7580
52. Rivadeneira J, Gorustovich A (2017) Bioactive glasses as delivery systems for antimicrobial agents. J Appl Microbiol 122(6):1424–1437
53. Schuhladen K, Stich L, Schmidt J, Steinkasserer A, Boccaccini AR, Zinser E (2020) Cu, Zn doped borate bioactive glasses: antibacterial efficacy and dose-dependent in vitro modulation of murine dendritic cells. Biomater Sci 8(8):2143–2155
54. Rodriguez O, Stone W, Schemitsch EH, Zalzal P, Waldman S, Papini M, Towler MR (2017) Titanium addition influences antibacterial activity of bioactive glass coatings on metallic implants. Heliyon 3(10):e00420
55. Berlutti F, Frioni A, Natalizi T, Pantanella F, Valenti P (2014) Influence of sub-inhibitory antibiotics and flow condition on *Staphylococcus aureus* ATCC 6538 biofilm development and biofilm growth rate: BioTimer assay as a study model. J Antibiot 67(11):763–769
56. Passos TF, Souza MT, Zanotto ED, de Souza CWO (2021) Bactericidal activity and biofilm inhibition of F18 bioactive glass against *Staphylococcus aureus*. Mater Sci Eng C 118:111475
57. Begum S, Johnson WE, Worthington T, Martin RA (2016) The influence of pH and fluid dynamics on the antibacterial efficacy of 45S5 Bioglass. Biomed Mater 11(1):015006
58. Souza M, Campanini L, Chinaglia C, Peitl O, Zanotto E, Souza C (2017) Broad-spectrum bactericidal activity of a new bioactive grafting material (F18) against clinically important bacterial strains. Int J Antimicrob Agents 50(6):730–733
59. da Silva LCA, Neto FG, Pimentel SSC, da Silva PR, Sato F, Retamiro KM, Fernandes NS, Nakamura CV, Pedrochi F, Steimacher A (2021) The role of Ag2O on antibacterial and bioactive properties of borate glasses. J Non-Cryst Solids 554:120611
60. Pandit A, Adholeya A, Cahill D, Brau L, Kochar M (2020) Microbial biofilms in nature: unlocking their potential for agricultural applications. J Appl Microbiol 129(2):199–211
61. Sheppard DC, Howell PL (2016) Biofilm exopolysaccharides of pathogenic fungi: lessons from bacteria. J Biol Chem 291(24):12529–12537
62. Coraça-Huber DC, Fille M, Hausdorfer J, Putzer D, Nogler M (2014) Efficacy of antibacterial bioactive glass S53P4 against *S. aureus* biofilms grown on titanium discs in vitro. J Orthop Res 32(1):175–177
63. Petříčková K, Chroňáková A, Zelenka T, Chrudimský T, Pospíšil S, Petříček M, Krištůfek V (2015) Evolution of cyclizing 5-aminolevulinate synthases in the biosynthesis of actinomycete secondary metabolites: outcomes for genetic screening techniques. Front Microbiol 6:814
64. Chang H-Y, Cang J, Roy P, Chang H-T, Huang Y-C, Huang C-C (2014) Synthesis and antimicrobial activity of gold/

silver–tellurium nanostructures. ACS Appl Mater Interfaces 6(11):8305–8312
65. Zhanel GG, Walters M, Laing N, Hoban DJ (2001) In vitro pharmacodynamic modeling simulating free serum concentrations of fluoroquinolones against multidrug-resistant Streptococcus pneumoniae. J Antimicrob Chemother 47:435–440
66. Ahmed A, Ali A, Mahmoud DA, El-Fiqi A (2011) Study on the preparation and properties of silver-doped phosphate antibacterial glasses (part I). Solid State Sci 13(5):981–992
67. Zare B, Faramarzi MA, Sepehrizadeh Z, Shakibaie M, Rezaie S, Shahverdi AR (2012) Biosynthesis and recovery of rod-shaped tellurium nanoparticles and their bactericidal activities. Mater Res Bull 47(11):3719–3725. https://doi.org/10.1016/j.materresbull.2012.06.034
68. Hu S, Chang J, Liu M, Ning C (2009) Study on antibacterial effect of 45S5 Bioglass®. J Mater Sci Mater Med 20(1):281–286
69. Abdelghany A, Behairy A (2020) Optical parameters, antibacterial characteristics and structure correlation of copper ions in cadmium borate glasses. J Market Res 9(5):10491–10497
70. Naseri S, Lepry WC, Maisuria VB, Tufenkji N, Nazhat SN (2019) Development and characterization of silver-doped sol-gel-derived borate glasses with anti-bacterial activity. J Non-Cryst Solids 505:438–446
71. Rau JV, De Bonis A, Curcio M, Schuhladen K, Barbaro K, De Bellis G, Teghil R, Boccaccini AR (2020) Borate and silicate bioactive glass coatings prepared by nanosecond pulsed laser deposition. Coatings 10(11):1105
72. Boschetto F, Ngoc Doan H, Phong Vo P, Zanocco M, Zhu W, Sakai W, Adachi T, Ohgitani E, Tsutsumi N, Mazda O (2020) Antibacterial and osteoconductive effects of chitosan/polyethylene oxide (PEO)/bioactive glass nanofibers for orthopedic applications. Appl Sci 10(7):2360
73. Cunha MT, Murça MA, Nigro S, Klautau GB, Salles MJC (2018) In vitro antibacterial activity of bioactive glass S53P4 on multiresistant pathogens causing osteomyelitis and prosthetic joint infection. BMC Infect Dis 18(1):1–6
74. Chen W, Liang J, He Z, Jiang W (2016) Preliminary study on total protein extraction methods from Enterococcus faecalis biofilm. Genet Mol Res 15 (10.4238)
75. Compton SJ, Jones CG (1985) Mechanism of dye response and interference in the Bradford protein assay. Anal Biochem 151(2):369–374
76. Wilkinson HN, Iveson S, Catherall P, Hardman MJ (2018) A novel silver bioactive glass elicits antimicrobial efficacy against *Pseudomonas aeruginosa* and *Staphylococcus aureus* in an ex vivo skin wound biofilm model. Front Microbiol 9:1450
77. Singh V, Phukan UJ (2019) Interaction of host and Staphylococcus aureus protease-system regulates virulence and pathogenicity. Med Microbiol Immunol 208(5):585–607
78. Modglin VC, Brown RF, Jung SB, Day DE (2013) Cytotoxicity assessment of modified bioactive glasses with MLO-A5 osteogenic cells in vitro. J Mater Sci Mater Med 24(5):1191–1199. https://doi.org/10.1007/s10856-013-4875-8
79. Rismanchian M, Khodaeian N, Bahramian L, Fathi M, Sadeghi-Aliabadi H (2013) In-vitro comparison of cytotoxicity of two bioactive glasses in micropowder and nanopowder forms. Iran J Pharm Res IJPR 12(3):437
80. Shoaib M, Bahadur A, Iqbal S, Al-Anazy MM, Laref A, Tahir MA, Channar PA, Noreen S, Yasir M, Iqbal A (2021) Magnesium doped mesoporous bioactive glass nanoparticles: a promising material for apatite formation and mitomycin c delivery to the MG-63 cancer cells. J Alloys Compd 866:159013
81. Shoaib M, Saeed A, Akhtar J, Rahman MSU, Ullah A, Jurkschat K, Naseer MM (2017) Potassium-doped mesoporous bioactive glass: synthesis, characterization and evaluation of biomedical properties. Mater Sci Eng, C 75:836–844